A collective form of cell death requires homeodomain interacting protein kinase

Nichole Link, Po Chen, Wan-Jin Lu, Kristi Pogue, Amy Chuong, Miguel Mata, Joshua Checketts, and John M. Abrams

Department of Cell Biology, UT Southwestern Medical Center, Dallas, TX 75390

We examined post-eclosion elimination of the *Drosophila* wing epithelium in vivo where collective "suicide waves" promote sudden, coordinated death of epithelial sheets without a final engulfment step. Like apoptosis in earlier developmental stages, this unique communal form of cell death is controlled through the apoptosome proteins, Dronc and Dark, together with the IAP antagonists, Reaper, Grim, and Hid. Genetic lesions in these pathways caused intervein epithelial cells to persist, prompting a characteristic late-onset blemishing phenotype throughout the wing blade. We leveraged this phenotype in mosaic animals to discover relevant genes and establish here that *homeodomain interacting protein kinase* (*HIPK*) is required for collective death of the wing epithelium. Extra cells also persisted in other tissues, establishing a more generalized requirement for HIPK in the regulation of cell death and cell numbers.

Introduction

Elimination of cells by programmed cell death (PCD) is a universal feature of development and aging (Jacobson et al., 1997; Vaux and Korsmeyer, 1999). In both vertebrates and invertebrates, dying cells often progress through a stereotyped set of transformations referred to as apoptosis. In this form of PCD the nucleus condenses, and the collapsing cell corpse fragments into "apoptotic bodies" that are engulfed by specialized phagocytes or neighboring cells (Kerr et al., 1972; Wyllie et al., 1980; Kerr and Harmon, 1991). Apoptosis requires autonomous genetic functions within the dying cell, and extrinsic cues that elicit apoptosis have been investigated in numerous experimental models (Danial and Korsmeyer, 2004; Salvesen and Abrams, 2004). Other forms of death are also thought to contribute during development and differ from apoptosis with respect to cellular morphology, mechanism, or mode of activation. These may include necrosis, characterized by swelling of the plasma membrane, or autophagic cell death, which is linked to extensive vacuolization in the cytoplasm (Kroemer et al., 2005). These forms of cell death can be caspase dependent or independent and may or may not be under deliberate genetic control (Kroemer et al., 2005).

Two conserved protein families comprise central elements of the apoptotic machinery (Salvesen and Abrams, 2004).

Orthologous proteins represented by Ced4 in the nematode, Apaf1 in mammals, and *Drosophila* Ark (Dark) function as activating adaptors for CARD-containing apical caspases. During apoptosis, Ced4/Apaf1/Dark adaptors associate with pro-caspase partners (Ced3, Caspase 9, and Dronc) in a multimeric complex referred to as the "apoptosome". This complex is regulated by Bcl2 proteins, but apparently through different mechanisms (for review see Kornbluth and White, 2005).

Previously, we and others genetically examined components of the *Drosophila* apoptosome (Rodriguez et al., 1999, 2002; Chew et al., 2004; Daish et al., 2004; Xu et al., 2005; Akdemir et al., 2006; Mills et al., 2006; Srivastava et al., 2006). *dark* and *dronc* are recessive, lethal genes. Both exert global functions during PCD and in stress-induced apoptosis. However, their roles in apoptosis are not absolute because rare cell deaths occurred in embryos lacking maternal and zygotic product of either gene (Xu et al., 2005; Akdemir et al., 2006). Elimination of *dronc* in the wing caused a unique, age-dependent phenotype associated with late-onset blemishing throughout the wing blade (Chew et al., 2004). Here, we show that this progressive phenotype is characteristic for wing epithelia that lack apoptogenic functions and is caused by defects in a communal form of PCD where epithelial cells are collectively and rapidly eliminated. We leveraged these findings to discover additional genes required for PCD and recovered a limited set of loci, many of which were previously unknown to function in cell death. Here, we establish that *homeodomain interacting protein kinase* (*HIPK*) is essential for coordinated death in the wing epithelium and, consistent with PCD functions in earlier

developmental stages, regulates proper cell number in diverse tissue types.

Results and discussion

Proper maintenance of the adult wing requires PCD gene activity

Wings mosaic for *dronc⁻* tissue exhibit normal morphology at eclosion but develop progressive, melanized blemishes with age (Chew et al., 2004). We applied similar methods to determine whether lesions in other apoptogenic genes present a similar phenotype. After eclosion, wings mosaic for *Df(H99)*, a deletion removing the apoptotic activators *reaper* (*rpr*), *grim*, and *hid* (Abrams, 1999), were morphologically normal at eclosion, but over 3–7 d, melanized blemishes appeared at random throughout the wing (Fig. 1 C). Likewise, homozygous *drice*^Δ1 adult "escapers" deficient for the effector caspase Drice (Muro et al., 2006) also presented normal wings at eclosion but developed blemishes with age (Fig. 1 D). Wings mosaic for *dark*^82, a null allele of *dark* (Akdemir et al., 2006), were indistinguishable from wild-type (WT) at eclosion (Fig. 1 A), but within 4 d developed wing blemishes (Fig. 1 B). These late-onset blemishes became markedly more severe as animals aged. Similar yet less severe wing blemishes occurred in adults homozygous for *dark*^CD4, a hypomorphic allele of *dark* (Chew et al., 2004). Together, these observations establish that late-onset progressive blemishing in mosaic wings is a characteristic phenotype shared among mutants in canonical PCD pathways.

The wing blemish phenotype results from a failure in epithelial PCD

In the wing of newly eclosed adults, PCD removes the epithelium that forms the dorsal and ventral cuticles (Johnson and Milner, 1987; Kimura et al., 2004). To determine whether the cause of the blemish phenotype might trace to defective death in the wing epithelium, we examined this tissue in *dark* mutants. For these studies, wings of *dark*^CD4 adults were prepared for light and electron microscopy. Histological analyses at the light level showed that on the first day of eclosion, the dorsal and ventral cuticles of WT animals became tightly merged with no intervening tissue evident between these layers (Fig. 1 E). However, even 14 d after eclosion, cells and cell remnants remained situated between the dorsal and ventral cuticles in *dark* mutants. This "undead" tissue was most easily visualized in lateral sections through melanized blemishes (Fig. 1, F–H). Further examination of the persisting epithelium at the EM level showed evidence of intact cells soon after eclosion (Fig. 1 P) and ectopic cellular material 24 h after eclosion (Fig. 1, I–K).
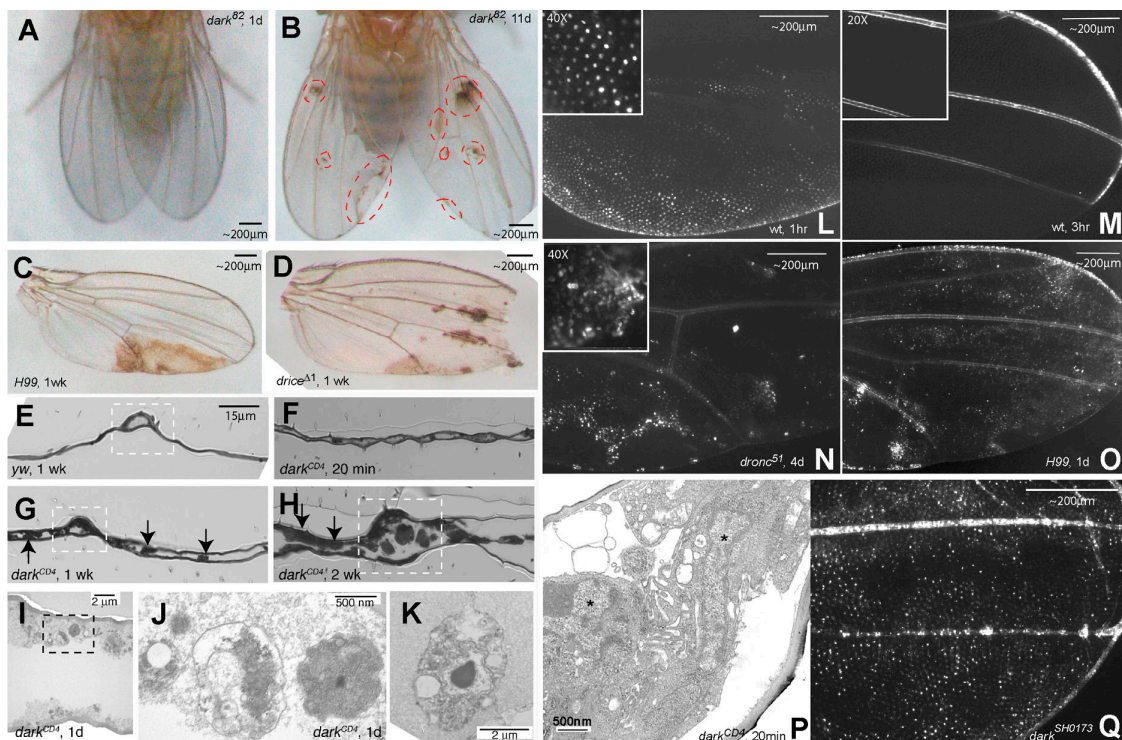

Figure 1. **Cell death–defective adult phenotypes in mosaic wings.** (A) Mosaic wings of animals bearing *dark*^82 clones have normal morphology 1 d (d) after eclosion. (B) The same adult as in panel A developed melanized blemishes (dotted circles) 11 d after eclosion. (C) Wings mosaic for *H99* and (D) *drice*^Δ1 7 d after eclosion. E–H are toluidine blue–stained plastic sections through the wings of WT (E) and *dark* mutants (F–H). Arrows (F–H) indicate ectopic tissue and cell remnants between the cuticle layers in *dark* mutants. Boxed regions in E, G, and H indicate wing veins. I–K and P are electron micrographs of persisting tissue in *dark*^cd4 wings, showing ultrastructure of intact cellular material, 1 d (I–K) and 20 min (P) post-eclosion. J is boxed region in I. Asterisk in P indicates the nucleus. (L) WT wing epithelium is visualized with *vg:DsRed* within 1 h of eclosion. By 2–3 h post-eclosion, these cells completely disappeared (panel M and Supplemental Videos, available at http://www.jcb.org/cgi/content/full/jcb.200702125/DC1). Wings that are mosaic for *dronc⁻* (N), *H99* (O), or *dark* (Q) retain persisting wing epithelial cells, shown here 4 d, 24 h, and at least 6 h after eclosion.

Live imaging reveals collective elimination of the wing epithelium

To directly examine the death of wing epithelial cells in vivo, we adapted a transgenic nuclear DsRed reporter driven by *vestigial-Gal4* (*vg:DsRed*) (Vegh and Basler, 2003; Barolo et al., 2004), which permits visualization of the fate of these cells soon after eclosion. Observations with this pan-epithelial marker in the wing confirmed earlier studies (Kimura et al., 2004; Xu et al., 2005). Fig. 1 L shows that within 1 h of eclosion, intact epithelial cells are clearly present and regularly patterned throughout the wing. 1–2 h later (2–3 h after eclosion), the entire intervein epithelium disappears, manifested here by the abrupt loss of DsRed throughout the wing blade (Fig. 1 M). Live, real-time imaging of the wing in newly eclosed adults revealed unexpected features associated with elimination of the intervein epithelium (Fig. 2 and Videos 1–3, available at http://www.jcb.org/cgi/content/full/jcb.200702125/DC1). Epithelial cells, labeled by nuclear fluorescence, were arranged in a regular, predictable pattern throughout the wing. Then, consistent with nuclear breakdown, fluorescence became redistributed throughout the cell followed by indications of blebbing and the appearance of fragmenting cells. Occasionally, weak fluorescence enclosed in cell corpses condensed to bright punctate bodies. This series of apoptogenic changes spread extremely rapidly throughout the epithelium, appearing here as a collective wave initiating from the peripheral edge and moving across the wing blade (Fig. 2, top panels). Within just 4 min, virtually all nuclei (~450 cells) within a space of ~114 mm^2 converted from viable to apoptotic morphology. The process involved tight coordination at the group level because the likelihood of a single cell apoptosing was clearly linked to similar behaviors by nearest neighboring cells over short time frames (Video 1). Also, the direction and size of the cell death wave may not be fixed in every region of the wing, but centrally located cell groups were generally eliminated earlier (Fig. 1 L).

Unlike conventional examples of PCD in development, we found no indication that overt engulfment of apoptotic corpses occurred at the site of death. Instead, DsRed-labeled cell remnants were passively swept *en masse* toward the nearest wing vein (Fig. 2, bottom panels) where, apparently under hydrostatic pressure, cell debris streamed proximally toward the body through the wing or along the wing vein (Fig. 2, bottom panels; and Video 3). Together, these observations describe a communal form of PCD that rapidly eliminates the wing epithelium through coordinated group behavior.

Cells mutated for genes in the cell death pathway persist in the wing epithelium

We used the *vg:DsRed* reporter to track the fate of mosaic wing epithelia where mutant clones were induced. In sharp contrast to WT wings, abnormally persisting cells could be readily detected as patches of DsRed in the nuclei of epithelial cells in mosaic tissues. For example, wings mosaic for *dronc⁻* clones retained extensive patches of persisting DsRed-labeled cells (Fig. 1 N). Here, cells and nuclei were readily detected 4 d after eclosion (Fig. 1 N), and even at 11 d post-eclosion, extensive evidence of cell debris was seen (not depicted). We found that wings mosaic for the *H99* deletion gave identical results (Fig. 1 O). Likewise, adults mutated for *dark* exhibited persisting cells throughout the wing blade (Fig. 1 Q). Consistent with this, rare *drice*$^{\Delta 1}$ escapers also showed evidence of persisting cells after eclosion (Muro et al., 2006). These observations link failures in PCD to progressive melanized wing blemishes, raising
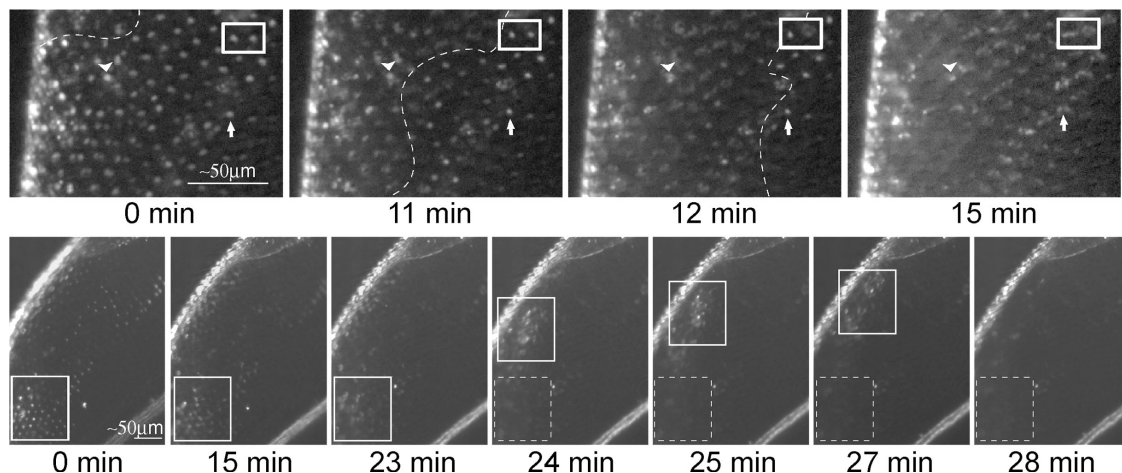

Figure 2. **Collective cell death eliminates the wing epithelium.** Time-lapse micrographs of *vg:DsRed* marked wings of newly eclosed adults (see Materials and methods). In the top panel, at 0 min, cells are intact. At 11 min, several cells lose nuclear localized fluorescent signal as fluorescence distributes throughout the cell consistent with nuclear breakdown and blebbing (arrowheads). 1 min later (12 min), apoptosis has occurred further away from the wing margin, and by 15 min, all cells have undergone PCD. The dotted line in 0, 11, and 12 min marks the progression of an "apoptotic wave" through the epithelium, and the box and arrows represent the same cells in each panel. At 11 min, both cells in the box are intact. However, at 12 min the right cell has clearly undergone PCD while the left cell remains intact. Finally, at 15 min both cells have lost their nuclear signal and have undergone PCD. The bottom panels depict intact cells at 0 min (box), but by 15 min cells have apoptosed and have begun movement toward the wing vein at 24 min. All cells are eliminated by 28 min. In these frames, the solid box follows the group of cells as they move while the dotted box marks the original location of the cells. Complete videos are available as supplemental material (http://www.jcb.org/cgi/content/full/jcb.200702125/DC1). Bottom frames are excerpts from Video 3, which were captured within 2 h after eclosion.

the possibility that other apoptogenic mutants might also produce this phenotype.

A phenocopy screen recovers new cell death–defective mutations

Unlike previously described wing defects, which are congenital and evident at eclosion (Lawrence, 1992; Lindsley and Zimm, 1992), the age-dependent phenotype described in Fig. 1 (A–D) is characteristic of mutations in genes that function in canonical PCD pathways. Moreover, when the dosage of *dronc* was reduced by half in *dark^{CD4}* adults (Chew et al., 2004) or if WT Dmp53 was removed from these same animals, melanized blemishes became far more severe. These genetic interactions are highly specific because wing defects were never observed in *Dmp53^−* homozygotes or in *dronc^{51}* heterozygotes (unpublished data). Numerous other mutants showed no such effects in combination with a *dark* hypomorph. We reasoned that, if genetically eliminated, additional regulators and effectors in PCD pathways should phenocopy wings mosaic for *dark^−* or *dronc^−* tissue. We screened a collection of preexisting transposon mutants to capture insertions that exhibit normal wings at eclosion but develop melanized blemishes with age. Our strategy exploits the FLP/FRT system together with wing-specific drivers to interrogate animals bearing wing genotypes mosaic for clones of P element–derived lethal mutations. Progeny with mosaic wings were examined for late-onset wing blemishes at 1, 7, and 14 d post-eclosion. We screened over 1,000 lethal insertions, representing 356 2nd chromosome mutations and 707 3rd chromosome mutations.

The majority of insertions (87%) produced no visible defects as wing mosaics (see online supplemental tables, available at http://www.jcb.org/cgi/content/full/jcb.200702125/DC1). 13% of insertions tested produced abnormalities, and these were scored for the phenotypic categories shown in Fig. S1. Congenital defects including notched, blistered, or wrinkled wings occurred alone or occasionally as compound phenotypes (Fig. S1, A–D). The candidate strains that developed wing blemishing were further subdivided based on phenotypic severity. Insertions in class A developed pronounced blemishes within a week of eclosion (Fig. S1 E), whereas those in class B developed relatively light-colored patches between 1 and 2 wk after eclosion (Fig. S1 F). Mutant lines exhibiting class A phenotypes were rare (∼2%). All members of this class lacked blemishes at eclosion and displayed progressive blemishing occasionally associated with fragile and sometimes broken wings (Fig. S1 E). A new allele of *dark* (l(2)SH0173) was recovered in this class (Table S2), providing reassuring validation for our screening strategy. Some members among these classes exhibited congenital notches or blisters, but congenital blemishes present at eclosion were not found.

We applied inverse PCR to map or confirm insertion sites of many class A and B strains (Table S2). In addition to
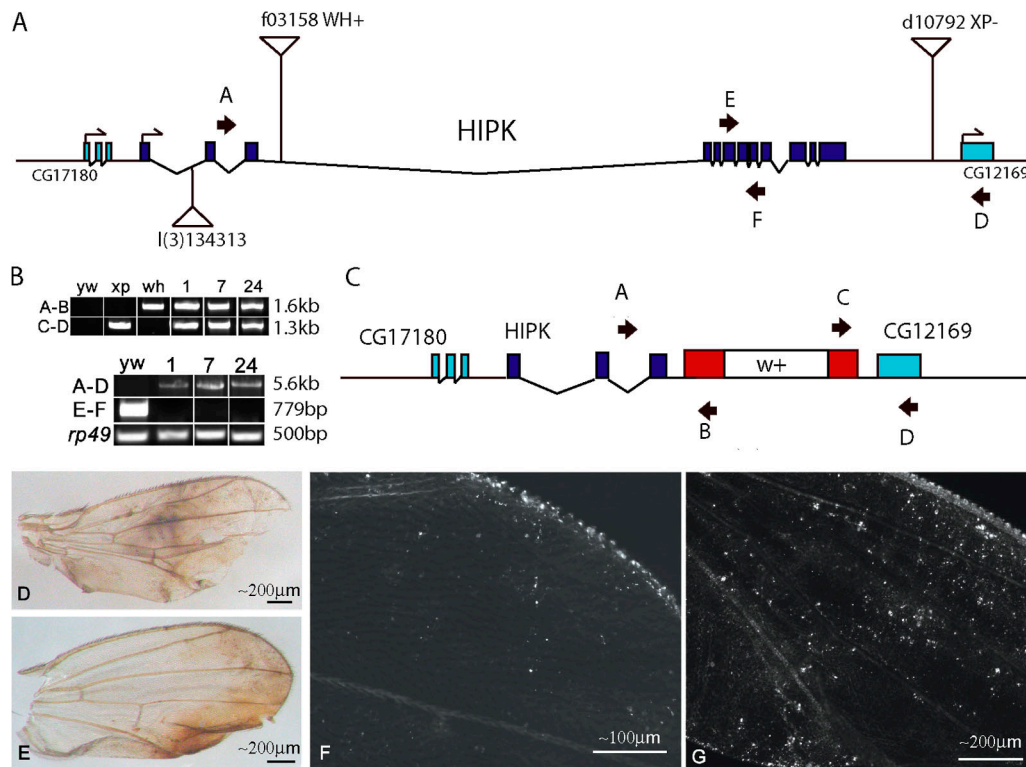

Figure 3. **HIPK is essential for normal PCD in the wing epithelium.** The *HIPK* locus is depicted (A) with the original insertion, l(3)S134313. Other transposons, *f03158* and *d10792*, were used to generate a deletion *HIPK^{D1}* (C), which removes 92% of the *HIPK* coding region by replacing residues 1–1243 of the *HIPK* coding sequences with *white+* marker gene. Primer sets A-B and C-D (C) were used to identify recombination events by genomic PCR. Deletions were verified in panel B using two additional primer sets, which resulted in a novel PCR product (primers A–D) and a negative PCR result (primers E-F) in homozygous mutant DNA. *rp49* represents a positive control. Wings mosaic for both *HIPK^{l(3)S134313}* (D and F) and *HIPK^{D1}* (E and G) were normal at eclosion, but upon aging showed severe blemishing and persisting cell phenotypes (D–G), with *HIPK^{D1}* wings exhibiting additional persisting DsRed cells (G). Note that the progressive blemishing phenotypes were not seen in parental strains, including those used to produce FRT recombinants.

dark[l(3)SH0173], we isolated several mutations associated with genes previously implicated in PCD (Table S1). For example, l(2)SH2275 contains an insertion 2 kb upstream of *mir-14*, a microRNA capable of modulating Rpr-induced cell death (Xu et al., 2003). Likewise, l(3)S048915 maps to the first intron of DIAP1 and may represent a hypermorphic allele at this locus. l(3)S055409 maps near *misshapen* (Su et al., 1998), a gene implicated in cell killing triggered by Rpr or Eiger, the fly counterpart of TNF (Igaki et al., 2002; Kuranaga et al., 2002). Several insertions map in or near transcriptional or translational regulators that might alter the expression of cell death genes. For example, *grunge* (l(3)S146907), an Atrophin-like protein (Erkner et al., 2002), functions as a transcriptional repressor (Zhang et al., 2002), while *belle* (l(3)S097074) belongs to the DEAD-box family of proteins (Johnstone et al., 2005) often implicated in translational regulation and RNA processing.

A portion of the class A and B hits were also directly examined for defective PCD by applying the *vg:DsRed* reporter in mosaic wings. Of the 29 strains tested, 14 showed obvious evidence for persisting cells in the wing epithelium (Table S2), which include dark[l(3)SH0173] (Fig. 1 Q).

HIPK is essential for normal PCD of the wing epithelium

Mutants identified above that exhibit both blemishing and persisting cells are likely candidates for PCD genes. One strain, l(3)S134313, produced severe late-onset blemishing (Fig. 3 D)

and a persisting cell phenotype (Fig. 3 F). After mapping this insertion to the first intron of the *HIPK*, we produced null alleles at this locus by a customized deletion strategy illustrated in Fig. 3. Two FRT-containing P element insertions flanking the coding region of *HIPK* (Fig. 3 A) were used to generate a novel deletion depicted in Fig. 3 C (see Materials and methods). PCR verified recombination between P elements (Fig. 3 B), and 8 deletion strains were recovered. These validated alleles eliminate exons 4–12, removing over 92% of coding sequence in the predicted *HIPK* open reading frame. Deletions at the *HIPK* locus were uniformly lethal before the 3rd instar stage. However, zygotic *HIPK* is not essential to complete embryogenesis because ~70% of *HIPK* homozygotes hatch to 1st instar larvae. *HIPK[D1]* was recombined on the FRT79 chromosome to generate adult wings mosaic for this allele, and like the original insertion, these animals also developed robust progressive blemishes (Fig. 3 E) and a persisting cell phenotype (Fig. 3 G). Both phenotypes were more severe than the original P insertion, suggesting that the l(3)S134313 allele is hypomorphic for *HIPK*. These findings link loss of *HIPK* function to our query phenotypes, establishing that the action of HIPK is essential for post-eclosion PCD in the wing epithelium.

HIPK affects neuronal cell numbers in the developing animal

Using general stains (acridine orange) or TUNEL methods, embryonic PCD was not overtly disturbed in *HIPK* mutants.
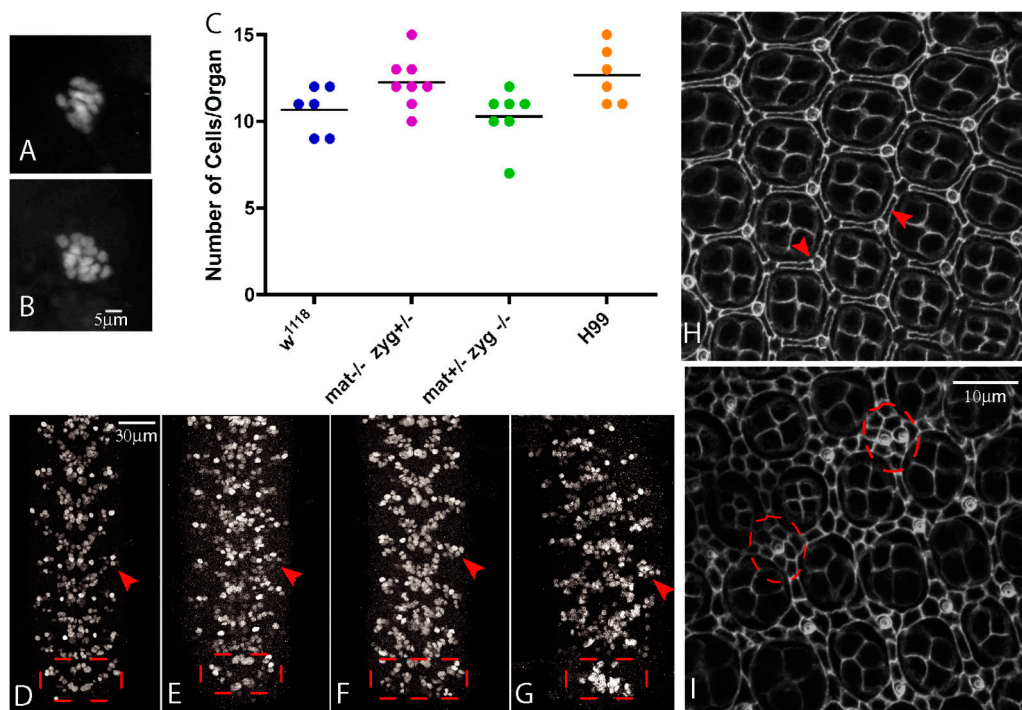

Figure 4. **Without *HIPK*, excessive neurons and cells are retained.** α-Kr Ab staining of Bolwig's organ precursors in WT (*w[1118]*) (A) and *HIPK* (B) mutants. The number of cells per organ is plotted in C. Note that zygotic *HIPK⁻* animals possess cell numbers equivalent to WT, but maternal *HIPK⁻* embryos have supernumerary cells comparable to levels seen in *H99* mutants. α-dHb9 Ab staining in *w[1118]* embryonic CNS filets shows the normal pattern of dHb9-positive cells in the ventral nerve cord at stage 16–17 (D). *HIPK* mutants at this same embryonic stage (E–G) show extra dHb9-positive cells and altered CNS patterning. Arrows and boxes indicate extra cells. The WT pattern of pupal eyes stained with α-Dlg is displayed in H with arrows illustrating interommatidial cells. *HIPK* mutant pupal eyes (I) exhibit more interommatidial cells (dotted lines), indicative of a defect in cell death. Distorted patterning of ommatidia and abnormal numbers of primary pigment cells were also seen in a subset of animals (not depicted).

To investigate the possibility of more subtle or specific phenotypes, we examined the nervous system using antibodies that label specific populations of neurons affected by the *H99* deletion (White et al., 1994). Using α-Kruppel antibody (Kosman et al., 1998), we confirmed that stage 14–15 WT embryos contained 9–12 Kruppel-positive cells in the Bolwig's Organ (Fig. 4, A and C). However, a portion of animals lacking maternal *HIPK* contained as many as 15 cells per organ (Fig. 4, B and C) at a penetrance comparable to *H99* animals, which are completely cell death defective (Fig. 4 C). We also examined neurons expressing dHb9, a homeodomain protein marking a subset of cells that persist in cell death–defective *H99* embryos (Rogulja-Ortmann et al., 2007). In germline clones, distinct classes of dHb9 staining patterns emerged. A subset of animals exhibited extreme patterning defects. Other animals displayed a striking increase in dHb9-positive cell numbers (Fig. 4, E–G) when compared with WT embryos of the parental strain (Fig. 4 D). These data establish that HIPK fundamentally regulates cell numbers in the nervous system, and because the same subpopulation of cells are affected by the *H99* mutation, they implicate HIPK as a more general regulator of PCD.

The pupal eye undergoes reorganization involving cell death of interommatidial cells after pupation (Wolff and Ready, 1991). To determine if HIPK regulates cell death in the retina, we generated whole eye clones and used the α-Dlg (discs large) antibody to outline cell borders in dissected pupal eyes after pupation. The WT pattern of interommatidial cells is represented in Fig. 4 H. In contrast, extra interommatidial cells were frequently retained in whole eye *HIPK⁻* clones (Fig. 4 I). This phenotype is overtly similar to animals lacking the apical caspase Dronc (Xu et al., 2005) and consistent with an essential role in retinal PCD.

Closing remarks

Elimination of the wing epithelium in newly eclosed adults is predictable, easily visualized, and experimentally tractable. The major histomorphologic events involve cell death, delamination, and clearance of corpses and cell remnants. Recent studies established that post-eclosion PCD is under hormonal control and involves the cAMP/PKA pathway (Kimura et al., 2004). While dying cells in the adult wing present apoptotic features (e.g., sensitivity to p35 and TUNEL positive), elimination of the epithelium is distinct from classical apoptosis in several important respects. First, unlike most in vivo models, overt engulfment of cell corpses does not occur at the site of death (Johnson and Milner, 1987; Ashkenas et al., 1996). Instead, dead or dying cells and their remnants are washed into the thoracic cavity via streaming of material along and through wing veins (Fig. 2, Videos 1–3; and Kimura et al., 2004). Second, extensive vacuolization is seen in ultrastructural analyses, which could indicate elevated autophagic activity (for review see Johnson and Milner, 1987; Kimura et al., 2004; and Fig. 1, I–K). Third, widespread and near synchronous death that occurs in this context defines an abrupt group behavior. The process affects dramatic change at the tissue level, causing wholesale loss of intervein cells and coordinated elimination of the entire layer of epithelium. Rather than die independently, these cells die communally, as if responding to coordinated signals propagated throughout the entire epithelium, perhaps involving intercellular gap junctions. This group behavior contrasts with canonical in vivo models where a single cell, surrounded by viable neighbors, sporadically initiates apoptosis.

One study proposed that an epithelial-to-mesenchymal transition (EMT) accounts for the removal of epithelial cells after eclosion (Kiger et al., 2007). Although our results do not exclude EMT associated changes in the newly eclosed wing epithelium, compelling lines of evidence, presented here and elsewhere, establish that post-eclosion loss of the wing epithelium occurs by PCD in situ—before cells are removed from the wing (Kimura et al., 2004). First, before elimination, wing epithelial cells label prominently with TUNEL. Second, every mutation in canonical PCD genes so far tested failed to effectively eliminate the wing epithelium (Fig. 1), and at least two of these were recovered in our screen. Third, elimination of the wing epithelium was reversed by induction of p35, a broad-spectrum caspase inhibitor (Kimura et al., 2004). Fourth, using time-lapse microscopy, we clearly detected condensing or pycnotic nuclei, followed by the rapid removal of all cell debris in time frames (minutes) not consistent with active migration. Instead, removal of cell remnants occurred by a passive streaming process, involving perhaps hydrostatic flow of the hemolymph.

Here, we sampled over one fifth of all lethal genes and nearly 10% of all genes in the fly genome for the progressive blemish phenotype, a reliable indicator of PCD failure in the wing epithelium. Nearly half of the mutants that produced melanized wing blemishing also displayed a cell death–defective phenotype when examined with the *vg:DsRed* reporter. The precise link between these defects is unclear, but a likely explanation suggests that as the surrounding cuticle fuses, persisting cells, now deprived for nutrients and oxygen, become necrotic and may initiate melanization. Mutants could arrest at upstream steps, involving the specification or execution of PCD, or they might affect proper clearance of cell corpses from the epithelium. We recovered new alleles of *dark* (l(2)SH0173) and a likely hypermorph of *thread* (l(3)S048915), which provides reassuring validation of this prediction.

By leveraging this distinct phenotype, we captured novel cell death genes, including the *Drosophila* orthologue of *HIPK*. Though first identified as an NK homeodomain binding partner (Kim et al., 1998), we found this gene to be an essential regulator of PCD and cell numbers in diverse tissue contexts. Of the four mammalian *HIPK* genes, *HIPK2*, the predicted orthologue of *Drosophila HIPK*, has been placed in the p53 stress-response apoptotic pathway (D'Orazi et al., 2002; Hofmann et al., 2002; Di Stefano et al., 2004, 2005), but whether the *Drosophila* counterpart similarly impacts this network is not yet known.

Materials and methods

Generation of mutant wing clones
The l(3)Sxxxxxx(Bellotto et al., 2002) and l(2)SHxxxx(Oh et al., 2003) FRT stocks were obtained from Szeged Stock Center. *vg-Gal4, UAS-FLP; FRT79, FRT82* and *vg-Gal4, UAS-FLP, FRT40, FRT42* were provided by K. Basler (University of Zürich, Zürich, Switzerland). *MS1096-Gal4, UAS-FLP* flies are from J. Jiang (UT Southwestern Medical Center, Dallas, TX). *FRT-Df(H99)*

stocks were provided by A. Gould (National Institute for Medical Research, London, UK) and J. O'Tousa (University of Notre Dame, Notre Dame, IN). To generate wing clones, 4 males of the genotype *l(3)Sxxxxxx-FRT82/TM3(6)* were crossed to 3 females of *vg-Gal4, UAS-FLP; FRT79, FRT82*. F1 flies were examined at eclosion and at 1 and 2 wk of age for appearance of "melanized blemishes" on the wing. *l(3)Sxxxxxx-FRT80/TM3(6)* and *l(2)SHxxxx-FRT40/Cyo* flies were similarly screened by crossing to *vg-Gal4:UAS-FLP; FRT80* and *vg-Gal4:UAS-FLP, FRT40, FRT42* flies, respectively. *MS1096-Gal4:UAS-FLP; FRT42B* was used for mutations on 2R. Adult wings were removed at different ages and fixed in paraformaldehyde for standard histology. Electron micrographs were generated using an electron microscope (TEMP2 1200 EX II; JEOL).

Detection of persisting wing epithelium
The FLP/FRT system was used to generate mutant wing clones, and persisting cells were visualized using DsRed. *UAS-RedStinger/Cyo; dronc^{51}-FRT79/TM6* was crossed to *vg-Gal4:UAS-FLP; FRT79, FRT82*. After eclosion, adults were aged from 1 to 14 d. Wings were removed, mounted on glass slides, and visualized using a fluorescent DLM (Axioplan; Carl Zeiss MicroImaging, Inc.) and a monochrome digital camera (Hamamatsu). *Df(H99)-FRT80, dark^{82}-FRT42D*, or *HIPK^{D1}-FRT79* lines with or without *UAS-RedStinger* were also crossed to their respective FLP/FRT lines and imaged as stated above. Epithelial cell death was recorded in time-lapse experiments using the previous crosses to image *w^{1118}; UAS-RedStinger/vg-Gal4, UAS-FLP; TM3(6)/FRT79* adults at 1–2 h after eclosion using a stereomicroscope (SteREO Discovery V.12; Carl Zeiss MicroImaging, Inc.) with Pentafluar S. Adults were glued on their dorsal surface to glass slides and imaged while alive. *UAS-RedStinger* lines were from Bloomington Stock Center.

Inverse PCR
P-element insertion sites were mapped by inverse PCR according to protocols from BDGP (http://www.fruitfly.org/about/methods/inverse.pcr.html). Genomic DNA of insertion lines containing the PlacW insertion element was extracted using Wizard Genomic DNA Extraction kit (Promega) and digested with HhaI, HpaII, and MboI restriction enzymes for 2.5 h at 37°C. Resulting digestions were diluted into 400 µl T4 DNA ligase (Roche) reactions and incubated overnight at 4°C. DNA was ethanol precipitated and used in Expand Long Template (Roche) PCR reactions with primers specific to the PlacW insertion. Unique PCR products were gel purified and sequenced, and insertion locations were confirmed using genomic PCR with primer sets specific to PlacW and surrounding genomic sequences.

HIPK deletion strains
Deletions were generated using the Exelixis collection of P elements as described previously (Parks et al., 2004; Thibault et al., 2004). To delete the *HIPK* locus, insertions *f03158* and *d10792* were placed in trans together with *hs-FLP* and heat-shocked to generate a FRT-mediated deletion. PCR primers directed to the remaining P elements and the surrounding genomic locus were used to identify deletion alleles (5′-TACTATTCCTTTCA-CTCGCACTTATTG-3′ and 5′-TAGATGAGGAAGTTCTGCGTGCAAGA-3′, 5′-CCTCGATATACAGACCGATAAAAC-3′ and 5′-CGACCTTCACCGACT-GATCCTGGAT-3′). Two additional primer pairs, one producing a novel PCR product spanning the deleted *HIPK* locus (5′-GTGTCACTCGAAATT-CGCCAGTGACT-3′ and 5′-GACGACTGACTCGGTAGCCTACTTCG-3′) while another specific to the deleted locus producing a negative result (5′-CGCTACTATCGTGCTCCCGAAATCAT-3′ and 5′-CGGATGCCTTGAC-ATTGTTGCAGT-3′), were used to confirm deletions.

Germline clones
Germline clones were generated using the dominant female sterile technique described previously (Chou et al., 1993; Chou and Perrimon, 1996).

Whole eye clones
HIPK^{D1}-FRT79/TM6 was crossed to *ey-FLP/Cyo; FRT79 GMR-Hid/TM6y+*, and pupated animals were removed and aged for 48–55 h. After aging, pupal eyes were dissected and fixed in 4% formaldehyde in PBS. Aged matched siblings carrying *TM6y+* were used as controls.

Immunohistochemistry
Immunohistochemistry was performed as described in Chew et al. (2004). Guinea pig α-Kruppel was used 1:600 (Kosman et al., 1998), rabbit α-dHb9 was used 1:500 (Broihier and Skeath, 2002), and α-Dlg was used 1:500 (Developmental Studies Hybridoma Bank) at 4°C overnight. Secondary antibodies used were labeled with Texas red or Fluorecein from Vector Laboratories (1:250) or Alexa 568 from Invitrogen (1:500). Genotyping was done using anti-GFP (1:1,000) from Invitrogen recognizing

GFP-labeled balancers. Confocal z-series were taken using a confocal microscope (TCS SP5; Leica) and used for counting. Z-series were stacked for presented images.

Microscopy
Adult wings were dry mounted, and images were acquired using a microscope (Stemi V6; Carl Zeiss MicroImaging, Inc.) equipped with a 1.0× lens using a digital camera (Coolpix5000; Nikon) or a stereomicroscope (SteREO Discovery V.12; Carl Zeiss MicroImaging) with PentafluarS using 0.63× or 1.5× PlanApoS lenses and an MRm or MRc5 digital camera (Axiocam) and Axiovision Release 4.6 software. Additional fluorescent wing images were acquired with a microscope (Axioplan 2E; Carl Zeiss MicroImaging, Inc.) and a monochrome digital camera (Hamamatsu) using Plan Neofluar 10×/0.30, Plan Apochromat 20×/0.60, and Plan Neofluar 40×/0.75 objectives and OpenLab software. Confocal images of tissues stained with Fluorescein and Alexa 568 were mounted in Vectashield (Vector Laboratories), and images were acquired on a confocal microscope (TCS SP5; Leica) with Leica LAS AF software. The following lenses were used: HC PL APO 20×/0.70, HCX PL APO 40×/1.25-0.75 oil, and HCX PL APO 63×/1.40-0.60 oil objectives. All images were taken at room temperature and were processed in ImageJ or Photoshop 7.0. Occasionally, images were linearly rescaled to optimize brightness and contrast uniformly without altering, masking, or eliminating data.

Online supplemental material
Fig. S1 displays the wing phenotypes characterized in the mosaic screen. Videos 1–3 are time-lapse experiments showing PCD of wing epithelial tissue taken as described in Materials and methods. Table S1 displays a summary of the P insertion wing mosaic screen, Table S2 lists loci implicated in coordinated death in the wing epithelium, and Table S3 is a summary of all strains screened. Online supplemental material is available at http://www.jcb.org/cgi/content/full/jcb.200702125/DC1.

References

Abrams, J.M. 1999. An emerging blueprint for apoptosis in *Drosophila*. *Trends Cell Biol.* 9:435–440.

Akdemir, F., R. Farkas, P. Chen, G. Juhasz, L. Medved'ova, M. Sass, L. Wang, X. Wang, S. Chittaranjan, S.M. Gorski, et al. 2006. Autophagy occurs upstream or parallel to the apoptosome during histolytic cell death. *Development*. 133:1457–1465.

Ashkenas, J., J. Muschler, and M.J. Bissell. 1996. The extracellular matrix in epithelial biology: shared molecules and common themes in distant phyla. *Dev. Biol.* 180:433–444.

Barolo, S., B. Castro, and J.W. Posakony. 2004. New *Drosophila* transgenic reporters: insulated P-element vectors expressing fast-maturing RFP. *Biotechniques*. 36:436–440, 442.

Bellotto, M., D. Bopp, K.A. Senti, R. Burke, P. Deak, P. Maroy, B. Dickson, K. Basler, and E. Hafen. 2002. Maternal-effect loci involved in *Drosophila* oogenesis and embryogenesis: P element-induced mutations on the third chromosome. *Int. J. Dev. Biol.* 46:149–157.

Broihier, H.T., and J.B. Skeath. 2002. *Drosophila* homeodomain protein dHb9 directs neuronal fate via crossrepressive and cell-nonautonomous mechanisms. *Neuron*. 35:39–50.

Chew, S.K., F. Akdemir, P. Chen, W.J. Lu, K. Mills, T. Daish, S. Kumar, A. Rodriguez, and J.M. Abrams. 2004. The apical caspase dronc governs programmed and unprogrammed cell death in *Drosophila*. *Dev. Cell*. 7:897–907.

Chou, T.B., and N. Perrimon. 1996. The autosomal FLP-DFS technique for generating germline mosaics in *Drosophila melanogaster*. *Genetics*. 144:1673–1679.

Chou, T.B., E. Noll, and N. Perrimon. 1993. Autosomal P[ovoD1] dominant female-sterile insertions in *Drosophila* and their use in generating germline chimeras. *Development*. 119:1359–1369.

D'Orazi, G., B. Cecchinelli, T. Bruno, I. Manni, Y. Higashimoto, S. Saito, M. Gostissa, S. Coen, A. Marchetti, G. Del Sal, et al. 2002. Homeodomain-interacting protein kinase-2 phosphorylates p53 at Ser 46 and mediates apoptosis. *Nat. Cell Biol.* 4:11–19.

Daish, T.J., K. Mills, and S. Kumar. 2004. *Drosophila* caspase DRONC is required for specific developmental cell death pathways and stress-induced apoptosis. *Dev. Cell.* 7:909–915.

Danial, N.N., and S.J. Korsmeyer. 2004. Cell death: critical control points. *Cell.* 116:205–219.

Di Stefano, V., G. Blandino, A. Sacchi, S. Soddu, and G. D'Orazi. 2004. HIPK2 neutralizes MDM2 inhibition rescuing p53 transcriptional activity and apoptotic function. *Oncogene.* 23:5185–5192.

Di Stefano, V., M. Mattiussi, A. Sacchi, and G. D'Orazi. 2005. HIPK2 inhibits both MDM2 gene and protein by, respectively, p53-dependent and independent regulations. *FEBS Lett.* 579:5473–5480.

Erkner, A., A. Roure, B. Charroux, M. Delaage, N. Holway, N. Core, C. Vola, C. Angelats, F. Pages, L. Fasano, and S. Kerridge. 2002. Grunge, related to human Atrophin-like proteins, has multiple functions in *Drosophila* development. *Development.* 129:1119–1129.

Hofmann, T.G., A. Moller, H. Sirma, H. Zentgraf, Y. Taya, W. Droge, H. Will, and M.L. Schmitz. 2002. Regulation of p53 activity by its interaction with homeodomain-interacting protein kinase-2. *Nat. Cell Biol.* 4:1–10.

Igaki, T., H. Kanda, Y. Yamamoto-Goto, H. Kanuka, E. Kuranaga, T. Aigaki, and M. Miura. 2002. Eiger, a TNF superfamily ligand that triggers the *Drosophila* JNK pathway. *EMBO J.* 21:3009–3018.

Jacobson, M.D., M. Weil, and M.C. Raff. 1997. Programmed cell death in animal development. *Cell.* 88:347–354.

Johnson, S.A., and J. Milner. 1987. The final stages of wing development in *Drosophila melanogaster*. *Tissue Cell.* 19:505–513.

Johnstone, O., R. Deuring, R. Bock, P. Linder, M.T. Fuller, and P. Lasko. 2005. Belle is a *Drosophila* DEAD-box protein required for viability and in the germ line. *Dev. Biol.* 277:92–101.

Kerr, J.F.R., and B.V. Harmon. 1991. Definition and incidence of apoptosis: an historical perspective. *In* Apoptosis: The Molecular Basis of Cell Death. Cold Spring Harbor Laboratory Press, New York. 5–29.

Kerr, J.F.R., A.H. Wyllie, and A.R. Currie. 1972. Apoptosis: a basic biological phenomenon with wide ranging implications in tissue kinetics. *Br. J. Cancer.* 26:239–257.

Kiger, J.A., Jr., J.E. Natzle, D.A. Kimbrell, M.R. Paddy, K. Kleinhesselink, and M.M. Green. 2007. Tissue remodeling during maturation of the *Drosophila* wing. *Dev. Biol.* 301:178–191.

Kim, Y.H., C.Y. Choi, S.J. Lee, M.A. Conti, and Y. Kim. 1998. Homeodomain-interacting protein kinases, a novel family of co-repressors for homeodomain transcription factors. *J. Biol. Chem.* 273:25875–25879.

Kimura, K., A. Kodama, Y. Hayasaka, and T. Ohta. 2004. Activation of the cAMP/PKA signaling pathway is required for post-ecdysial cell death in wing epidermal cells of *Drosophila melanogaster*. *Development.* 131:1597–1606.

Kornbluth, S., and K. White. 2005. Apoptosis in *Drosophila*: neither fish nor fowl (nor man, nor worm). *J. Cell Sci.* 118:1779–1787.

Kosman, D., S. Small, and J. Reinitz. 1998. Rapid preparation of a panel of polyclonal antibodies to *Drosophila* segmentation proteins. *Dev. Genes Evol.* 208:290–294.

Kroemer, G., W.S. El-Deiry, P. Golstein, M.E. Peter, D. Vaux, P. Vandenabeele, B. Zhivotovsky, M.V. Blagosklonny, W. Malorni, R.A. Knight, et al. 2005. Classification of cell death: recommendations of the Nomenclature Committee on Cell Death. *Cell Death Differ.* 12(Suppl 2):1463–1467.

Kuranaga, E., H. Kanuka, T. Igaki, K. Sawamoto, H. Ichijo, H. Okano, and M. Miura. 2002. Reaper-mediated inhibition of DIAP!-induced DTRAF degradation results in activation of JNK in *Drosophila*. *Nat. Cell Biol.* 4:705–710.

Lawrence, P.A. 1992. The Making of a Fly: The Genetics of Animal Design. Blackwell Scientific Publications, London. 240 pp.

Lindsley, D.L., and G.G. Zimm. 1992. The Genome of *Drosophila melanogaster*. Academic Press, San Diego. 1133 pp.

Mills, K., T. Daish, K.F. Harvey, C.M. Pfleger, I.K. Hariharan, and S. Kumar. 2006. The *Drosophila melanogaster* Apaf-1 homologue ARK is required for most, but not all, programmed cell death. *J. Cell Biol.* 172:809–815.

Muro, I., D.L. Berry, J.R. Huh, C.H. Chen, H. Huang, S.J. Yoo, M. Guo, E.H. Baehrecke, and B.A. Hay. 2006. The *Drosophila* caspase Ice is important for many apoptotic cell deaths and for spermatid individualization, a non-apoptotic process. *Development.* 133:3305–3315.

Oh, S.W., T. Kingsley, H.H. Shin, Z. Zheng, H.W. Chen, X. Chen, H. Wang, P. Ruan, M. Moody, and S.X. Hou. 2003. A P-element insertion screen identified mutations in 455 novel essential genes in *Drosophila*. *Genetics.* 163:195–201.

Parks, A.L., K.R. Cook, M. Belvin, N.A. Dompe, R. Fawcett, K. Huppert, L.R. Tan, C.G. Winter, K.P. Bogart, J.E. Deal, et al. 2004. Systematic generation of high-resolution deletion coverage of the *Drosophila melanogaster* genome. *Nat. Genet.* 36:288–292.

Rodriguez, A., H. Oliver, H. Zou, P. Chen, X.D. Wang, and J.M. Abrams. 1999. Dark is a *Drosophila* homologue of Apaf-1/CED-4 and functions in an evolutionarily conserved death pathway. *Nat. Cell Biol.* 1:272–279.

Rodriguez, A., P. Chen, H. Oliver, and J.M. Abrams. 2002. Unrestrained caspase-dependent cell death caused by loss of Diap1 function requires the *Drosophila* Apaf-1 homolog, Dark. *EMBO J.* 21:2189–2197.

Rogulja-Ortmann, A., K. Luer, J. Seibert, C. Rickert, and G.M. Technau. 2007. Programmed cell death in the embryonic central nervous system of *Drosophila melanogaster*. *Development.* 134:105–116.

Salvesen, G.S., and J.M. Abrams. 2004. Caspase activation—stepping on the gas or releasing the brakes? Lessons from humans and flies. *Oncogene.* 23:2774–2784.

Srivastava, M., H. Scherr, M. Lackey, D. Xu, Z. Chen, J. Lu, and A. Bergmann. 2006. ARK, the Apaf-1 related killer in *Drosophila*, requires diverse domains for its apoptotic activity. *Cell Death Differ.* 14:92–102.

Su, Y.C., J.E. Treisman, and E.Y. Skolnik. 1998. The *Drosophila* Ste20-related kinase misshapen is required for embryonic dorsal closure and acts through a JNK MAPK module on an evolutionarily conserved signaling pathway. *Genes Dev.* 12:2371–2380.

Thibault, S.T., M.A. Singer, W.Y. Miyazaki, B. Milash, N.A. Dompe, C.M. Singh, R. Buchholz, M. Demsky, R. Fawcett, H.L. Francis-Lang, et al. 2004. A complementary transposon tool kit for *Drosophila melanogaster* using P and piggyBac. *Nat. Genet.* 36:283–287.

Vaux, D.L., and S.J. Korsmeyer. 1999. Cell death in development. *Cell.* 96:245–254.

Vegh, M., and K. Basler. 2003. A genetic screen for hedgehog targets involved in the maintenance of the *Drosophila* anteroposterior compartment boundary. *Genetics.* 163:1427–1438.

White, K., M. Grether, J.M. Abrams, L. Young, K. Farrell, and H. Steller. 1994. Genetic control of programmed cell death in *Drosophila*. *Science.* 264:677–683.

Wolff, T., and D.F. Ready. 1991. Cell death in normal and rough eye mutants of *Drosophila*. *Development.* 113:825–839.

Wyllie, A.H., J.F.R. Kerr, and A.R. Currie. 1980. Cell death: the significance of apoptosis. *Int. Rev. Cytol.* 68:251–306.

Xu, D., Y. Li, M. Arcaro, M. Lackey, and A. Bergmann. 2005. The CARD-carrying caspase Dronc is essential for most, but not all, developmental cell death in *Drosophila*. *Development.* 132:2125–2134.

Xu, P., S.Y. Vernooy, M. Guo, and B.A. Hay. 2003. The *Drosophila* microRNA Mir-14 suppresses cell death and is required for normal fat metabolism. *Curr. Biol.* 13:790–795.

Zhang, S., L. Xu, J. Lee, and T. Xu. 2002. *Drosophila* atrophin homolog functions as a transcriptional corepressor in multiple developmental processes. *Cell.* 108:45–56.